Report on a problem studied at the UK Mathematics-in-Medicine Study Group Loughborough 2008
< http://www.maths-in-medicine.org/uk/2008/shaken-baby/ >

Solid-fluid interaction in force and energy transmission in shaken baby syndrome

Problem presented by Donal McNally

Report prepared by Rosemary Dyson, Gareth Jones
Leah Band and Bindi Brook.

May 7, 2009

1 Introduction

Cases of suspected shaken baby syndrome are difficult to diagnose due to a lack of scientific evidence. Current injury thresholds for shaken baby syndrome are empirical combinations of angular velocity and angular acceleration based on single-cycle shaking events. These thresholds are nearly impossible to exceed by shaking a baby, yet injuries are reported resulting from such abuse. This disparity between threshold and injury has led to controversy in the courts.

A diagram of the simplified head geometry is given in Figure 1. The brain and skull are separated by a thin layer of cerebrospinal fluid (CSF), but are attached via bridging vessels and the optic and aural nerves. Symptoms of shaken baby syndrome include loss of brain material integrity, subdural haematoma caused by rupture of the bridging vessels, and retinal bleeding. How shaking leads to these symptoms is currently unclear.

When cases of shaken baby syndrome present, there is often no history of the shaking event which caused it; there is therefore a lack of experimental evidence on shaking events and the damage they cause. Wolfson et al. [9] measured frequencies achieved during realistic shaking events, using an anthropomorphic test dummy. They found typical shaking frequencies of the order of $2.5 - 5$ Hz, and peak angular velocities and accelerations to be too low to cause damage based on scaled single-cycle injury thresholds found for the automotive industry. However, shaken baby syndrome consists of low-energy cyclic loading, and so these high-energy single event injury thresholds may not be appropriate to use; there is the possibility for energy accumulation and resonance.

We aim to predict whether a shaking event can lead to the damage observed clinically. During the study group we investigated two different mechanisms for brain damage during shaken baby syndrome: those caused by the elastic deformation of the brain, and those caused by the presence of the viscous CSF layer leading to rupture of bridging vessels.

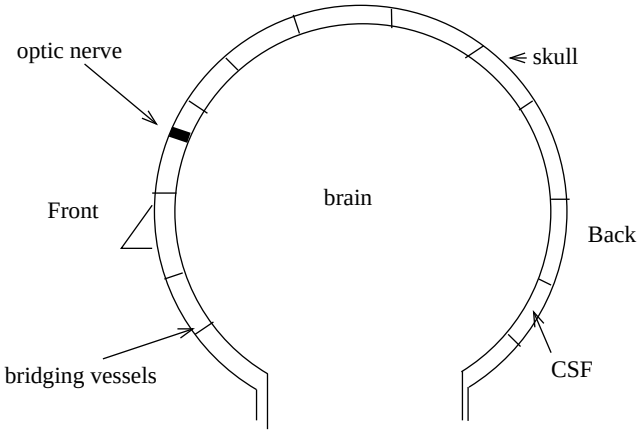

Figure 1: A schematic of the simplified head geometry.

We first consider the brain to be an incompressible linearly-elastic structure; in this case the motion of shaking can be decomposed into a longitudinal and a rotational part, which may then be considered separately. The effect of the thin layer of CSF within this model is captured by allowing tangential slip along the brain-skull boundary, whilst enforcing zero penetration. We investigate which of the decomposed motions will cause the largest deformation, and calculate the frequencies at which resonance within the brain will occur.

We then consider the dynamics of the CSF layer. Representing the brain and skull as square, rigid bodies with the brain contained within the skull, surrounded by a thin layer of CSF, we analyse the fluid dynamics of the CSF layer to find the variations in CSF thickness caused by oscillations of the skull. This is turn can be used to investigate whether the bridging vessels which attach the brain to the skull are likely to rupture.

2 Damage through elastic mechanisms

The pattern of damage displayed in the brain [2] is likely to be caused by large shear strains in the brain, as opposed to volumetric deformations, given that the brain is almost incompressible. However, the magnitude of the motions induced in a shaking event are unlikely to cause the large deformations required for such damage to take place. We must therefore investigate whether the cyclical nature of the shaking can give rise to resonant effects at certain frequencies, where excitation of the brain tissue at certain discrete frequencies causes the strain field in the brain to grow unboundedly.

2.1 Basic modelling

For simplicity, and to allow us to obtain representative analytical results, we model the brain as a linearly elastic solid [3], and take the CSF-layer thickness to be negligible. The displacement field $\boldsymbol{u}$ in such a material is given by the solution to Navier's equation,

$$(\lambda + G)\boldsymbol{\nabla}(\boldsymbol{\nabla} \cdot \boldsymbol{u}) + G\nabla^2 \boldsymbol{u} + \boldsymbol{f} = \rho \frac{\partial^2 \boldsymbol{u}}{\partial t^2}, \tag{1}$$

where λ and G are the Lamé material constants, $\boldsymbol{f}$ is a body force and ρ is the density of the solid. In the incompressible limit, the constant λ tends to infinity and $\boldsymbol{\nabla} \cdot \boldsymbol{u} = 0$. The Lagrangian multiplier associated with this constraint is the hydrostatic pressure p, and (1) becomes

$$G\nabla^2 \boldsymbol{u} - \boldsymbol{\nabla} p + \boldsymbol{f} = \rho \frac{\partial^2 \boldsymbol{u}}{\partial t^2}. \tag{2}$$

The boundary conditions that will be applied to this equation are

$$\boldsymbol{u} \cdot \boldsymbol{n} = 0, \tag{3}$$

$$(\boldsymbol{\sigma n}) \cdot \boldsymbol{t} = 0. \tag{4}$$

The first of these represents zero normal displacement, or the requirement that the brain does not penetrate the (assumed to be rigid) skull. The second condition, zero tangential traction, supposes that the cerebrospinal fluid layer (CSF) is inviscid and does not transmit shear stresses to the brain. In this latter expression $\boldsymbol{\sigma}$ is the stress tensor in the brain, given (for an incompressible material) by

$$\sigma_{ij} = -p\delta_{ij} + G\left(\frac{\partial u_i}{\partial x_j} + \frac{\partial u_j}{\partial x_i}\right) \tag{5}$$

in Cartesian coordinates, where δ_{ij} is Kronecker's delta.

One of the main advantages of linear elasticity is that the sum of two solutions to (1) [or to (2)] is also a solution of the relevant equation, by linearity. Thus we can decompose the motion caused by the shaking of the head into two canonical motions, and consider these motions separately. The typical head motion in a shaking event is a nodding of the head backwards and forwards. It is not hard to see that this motion can be decomposed into a unidirectional motion and a rotational motion, as indicated in Figure 2. We will construct Navier's equation in the frame of reference of the skull, in which the motion manifests itself as a body force $\boldsymbol{f}$.

As discussed above, these motions will now be treated separately to elucidate their effects on the brain. In both cases a spherical brain geometry will be selected in order to simplify the equations and obtain a representative result.

2.2 Unidirectional motion

We will first look at unidirectional motion. In this scenario the body force $\boldsymbol{f}$ does not vary in space. Solutions of the *compressible* static linear elastic

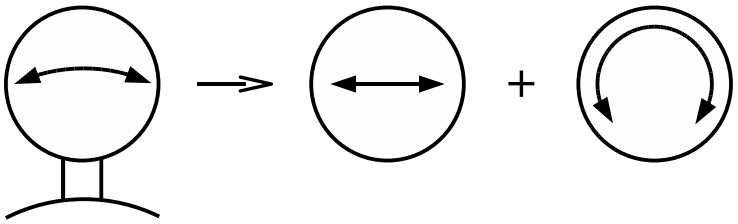

Figure 2: A diagram noting how a typical shaking motion (left) may be decomposed into a longitudinal and a rotational motion.

equations with a body force in a sphere have been given by [5]. Applying these solutions to the static problem gives rise to a solution which tends to zero in the incompressible limit $\lambda \to \infty$, the body force being completely balanced by the hydrostatic pressure. A glance at (2) reveals why. For a non-zero, uniform-in-space (but not necessarily constant in time) body force $\boldsymbol{f}$, the equations and corresponding boundary conditions are completely satisfied by the solution $\boldsymbol{u} = \boldsymbol{0}$, $p = \boldsymbol{f} \cdot \boldsymbol{x}$, where $\boldsymbol{x}$ is the position vector. This is true *whatever* the shape of the brain, since the stress in the brain is purely hydrostatic and thus acts only normal to the skull, so that (4) is satisfied.

In conclusion, considering only the brain tissue, a unidirectional shaking motion will not generate the magnitude of displacement necessary in order to create damage. For this, we must consider shear deformations.

2.3 Rotational shearing

Rotational shear motion, as indicated in Figure 2, is the only component of a typical shaking event that can cause damage, if one supposes (as shown in the previous section) that the effect of unidirectional motion is negligible. The proposed mechanism is resonance, where excitation of the brain tissue in rotational shear at a particular frequency allows the strains in the tissue to grow unboundedly, causing the type of damage seen in affected brains. To identify the frequencies at which resonance can occur, we take the time-dependent Navier equation (1) with zero body force $\boldsymbol{f} = \boldsymbol{0}$, suppose that $\boldsymbol{u} = \hat{\boldsymbol{u}}\, \mathrm{e}^{\mathrm{i}\omega t}$ and search for the eigenvalues ω of the equation. Then solving the equation with a shear body force varying sinusoidally at that frequency would give rise to an ever-growing strain field.

This problem has been studied by McClung [6]. That analysis was for compressible elasticity, but the results will be the same for incompressible elasticity if we restrict our analysis to motions which are equivoluminal (*i.e.* for which $\boldsymbol{\nabla} \cdot \boldsymbol{u} = 0$). McClung decomposed the motions into a linear combination of vector spherical harmonics, of which there were three types. Of those, the equivoluminal motions are described by motions which are linear combinations

of

$$\boldsymbol{X}_{nm} = -\frac{1}{\sqrt{n(n+1)}}\left[m\,\mathrm{cosec}\,\theta\, Y_n^m(\theta,\phi)\boldsymbol{e}_\theta + \mathrm{i}\frac{\partial Y_n^m}{\partial\theta}\,\boldsymbol{e}_\phi\right], \tag{6}$$

for $n = 1, 2, \ldots$ and $m = -n, \ldots, n$, where $Y_n^m(\theta,\phi)$ are surface spherical harmonics. Thus we let

$$\boldsymbol{u} = \mathrm{e}^{\mathrm{i}\omega t}\sum_{n=1}^{\infty}\sum_{m=-n}^{n} F_{nm}(r)\boldsymbol{X}_{nm}(\theta,\phi), \tag{7}$$

and substitute into (1) with $\boldsymbol{f} = \boldsymbol{0}$, to find

$$r^2F_{nm}'' + 2rF_{nm}' + \left[\frac{\omega^2r^2}{c_s^2} - n(n+1)\right]F_{nm} = 0, \tag{8}$$

where $c_s = \sqrt{G/\rho}$ is the shear wave speed in the material.

Solutions of (8) are readily found to be spherical Bessel functions,

$$F_{nm}(r) = c_{nm}j_n(\omega r/c_s) + d_{nm}y_n(\omega r/c_s). \tag{9}$$

We may set $d_{nm} = 0$ to avoid a singularity at $r = 0$. Thus

$$\boldsymbol{u} = \mathrm{e}^{\mathrm{i}\omega t}\sum_{n=1}^{\infty}\sum_{m=-n}^{n} c_{nm}j_n(\omega r/c_s)\boldsymbol{X}_{nm}(\theta,\phi). \tag{10}$$

Boundary conditions to (10) must now be applied at the outer boundary $r = r_0$, thus giving us the values of ω that correspond to resonant frequencies. If, in contrast to (3)–(4), a zero displacement condition $\boldsymbol{u} = \boldsymbol{0}$ was applied to (10), the orthogonality of $\boldsymbol{X}_{nm}$ for each n and m implies that the resonant frequencies are those for which

$$j_n(\omega r_0/c_s) = 0. \tag{11}$$

On the other hand, application of the zero tangential traction condition means that (10) must be substituted into (4).[1] Applying this condition, we require that

$$\left[\frac{\mathrm{d}}{\mathrm{d}r}j_n(\omega r/c_s) - \frac{1}{r}j_n(\omega r/c_s)\right]\Bigg|_{r=r_0} = 0. \tag{12}$$

By employing recurrence relations for spherical Bessel functions, it may be shown that this condition is equivalent to

$$(n-1)j_{n-1}(\omega r_0/c_s) - (n+2)j_{n+1}(\omega r_0/c_s) = 0. \tag{13}$$

The rotational motion indicated in Figure 2 is a combination of forcings of type $\boldsymbol{X}_{1,0}$. Thus, we must set $n = 1$ in the conditions (11) and (13), and

[1] Condition (3) is automatically satisfied by the fact that $\boldsymbol{X}_{nm}$ has no component in the $\boldsymbol{e}_r$ direction.

we obtain $j_1(\omega r_0/c_s) = 0$ for zero displacement and $j_2(\omega r_0/c_s) = 0$ for zero traction. Tables of the roots of spherical Bessel functions can be found, for instance, in [1]. The smallest (strictly positive) roots of $j_1(z)$ and $j_2(z)$ are $z_1 = 4.49$ and $z_2 = 5.76$ respectively. Thus, for zero displacement ($i = 1$) or for zero traction ($i = 2$) boundary conditions, the lowest resonant frequencies are given by $\omega = c_s z_i / r_0$.

In order to find representative numerical values for these resonant frequencies, we need to know the characteristic radius, density and shear modulus of the infant brain. We choose the density to be that of water, so that $\rho = 1000\,\mathrm{kg\,m^{-3}}$. Shear modulus values in the literature can vary by an order of magnitude, depending on the test used [4]. For vibrational testing at frequencies of $\sim 1\,\mathrm{Hz}$, measurements of the shear modulus range from 100 Pa to 3000 Pa, and a similar spread occurs for static loading. At higher frequencies, shear moduli of up to 30 kPa may be found. Other than frequency-dependent effects, the wide range of values may be explained by different experimental conditions, including sample thickness, temperature, brain anisotropy, the attachment of the sample to the measuring device, and measurement of different parts of the brain.

We will use the shear moduli determined by Hrapko *et al.* [4] for porcine brains, given by a representative value of $G \sim 300\,\mathrm{Pa}$. Thus the shear wave speed is given by $c_s = \sqrt{G/\rho} \sim 0.55\,\mathrm{m\,s^{-1}}$. For a typical brain radius of 5 cm, we thus have $\omega \sim 10.95 z_i$, or $\omega \sim 49.2\,\mathrm{rad\,s^{-1}}$ for zero-displacement boundary conditions and $\omega \sim 63.1\,\mathrm{rad\,s^{-1}}$ for zero-traction conditions. The resonant frequency f can be found from the angular frequency ω by $\omega = 2\pi f$, so that for zero-displacement and zero-traction boundary conditions the lowest resonant frequencies are 7.8 Hz and 10.0 Hz respectively.

2.4 Discussion

In this section we have looked at possible damage caused by elastic mechanisms. In particular, we have found that purely linear motion will not cause significant deformation, therefore the shearing damage noted in [2] can only be caused by rotational motion. This observation was somewhat confirmed by a empirical experiment performed at the study group, where a hemispherical bowl containing jelly, with water lubrication around the edges, was vibrated longitudinally and rotationally. A much greater deformation was seen for rotational motions, confirming the results of Section 2.2.

The second result from this section was to calculate the frequencies which gave rise to resonance in rotational shearing motions. The obtained values of 7–10 Hz seem to be inordinately large; however, they are at most four times the experimentally-determined values for shaking an anthropometric test dummy which lie in the range 2.5–5.0 Hz [9]. Eigenvalue computations are heavily dependent on the geometry of the domain being considered. Thus, it may be that various simplifications that we have made in terms of geometry, boundary conditions and material law may account for the overestimation in resonant frequency.

In particular, the brain displays highly viscoelastic behaviour in dynamic

(vibrational) testing. While such tests, as noted above, give a wide variety of elastic shear moduli depending on the test, there is also a significant viscoelastic part. The response of a linear viscoelastic material is characterised by a dynamic (or complex) modulus [8], the real part (the *storage modulus*) representing the elastic response and the imaginary part (the *loss modulus*) the viscous response. A purely elastic material has a real modulus while a purely viscous material would have an imaginary modulus. In the study of Hrapko *et al.* [4], the dynamic modulus is found to be around $300\,\mathrm{Pa} + 100\mathrm{i}\,\mathrm{Pa}$. Thus we could expect the viscosity of the brain tissue to play a significant role in its resonant behaviour. However, the main effect, we hypothesise, would be to attenuate the vibrations at the resonant frequencies, and not greatly change the frequencies at which resonance occurs.

Further analysis in these calculations should therefore consist of applying the calculations above to more realistic brain geometries, which would require the application of numerical methods. Additionally, further study of the mechanical properties of brain tissue must be carried out, in order to resolve the large difference in experimentally measured brain-tissue stiffnesses.

3 Fluid model

We now consider the movement of the CSF, which lies between the brain and the skull, to determine the displacement of the brain relative to the skull during a prescribed shaking event. Blood vessels bridge the gap between the brain and the skull, and shaken baby syndrome is often associated with rupture of these bridging vessels. By investigating the brain displacement, we can determine the stretching of the bridging vessels, and predict whether they are likely to rupture during a shaking event.

3.1 Model description

We investigate the fluid dynamics of the thin CSF layer which lies between the brain and the skull. For simplicity, we consider a horizontal plane through the head, and suppose that the brain and the skull are square and rigid, as shown on figure 3. We denote the length and width of the skull by $2L^*$ and the equilibrium thickness of the CSF layer by h_0^* (where asterisks are used to denote dimensional quantities throughout), and we assume $h_0^* \ll L^*$. The brain has density ρ_B^*, and the CSF has viscosity μ^* and density ρ_F^*. We assume that shaking causes the position of the skull to oscillate with a prescribed frequency, ω^*, [2] and prescribed amplitude, A^*, which is much greater than the CSF thickness, $A^* \gg h_0^*$. As the skull moves forward and backwards, the relative brain position displaces, resulting in a CSF thickness of $h_0^* + h^*(t^*)$ at the front of the head, and a CSF thickness of $h_0^* - h^*(t^*)$ at the back of the head. The thickness of the CSF at the sides of the brain is constant, h_0^* and we assume symmetry in the sagittal plane

[2] Note (in contrast to Section 2) that ω^* is the number of cycles per unit time, not the angular frequency.

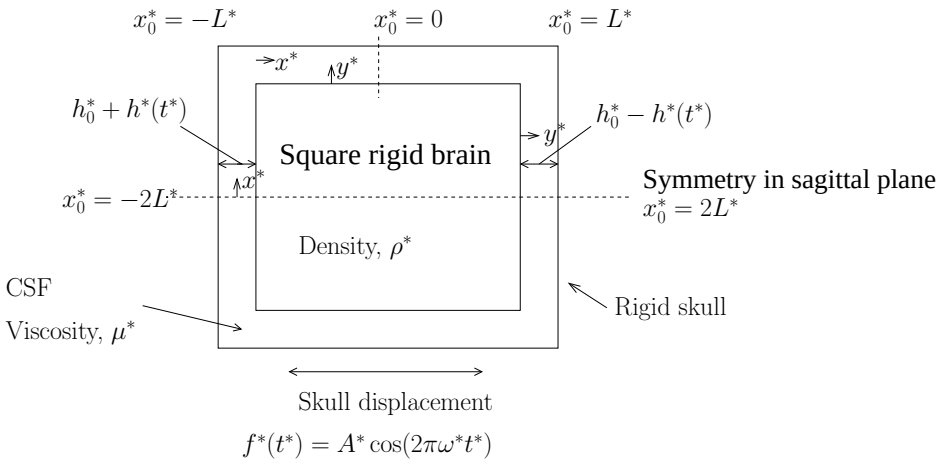

Figure 3: We investigate the movement of the CSF which lies between the brain and the skull, assuming that the brain and the skull are square and rigid. We prescribe the frequency and amplitude of skull displacement, and determine the relative brain displacement.

Parameter	Description	Value
h_0^*	Equilibrium CSF thickness	1 mm
L^*	Half brain length	0.05 m
μ^*	CSF viscosity	10^{-3} kg/(m s)
ρ_F^*	CSF density	10^3 kg/m^3
ρ_B^*	Brain density	10^3 kg/m^3

Table 1: Dimensional parameters estimates

(*i.e.* a vertical plane through the nose). We let x^* measure the length along the CSF layer, with $x^* = -2L^*$ corresponding to the nose position, and $x^* = 2L^*$ to the centre of the back of the head, and let y^* be the coordinate normal to the brain surface . We denote the CSF pressure and fluid velocities in the x^*, y^* direction at the front of the brain by $p_f^*(x^*, y^*, t^*)$, $u_f^*(x^*, y^*, t^*)$, $v_f^*(x^*, y^*, t^*)$, at the back of the brain by $p_b^*(x^*, y^*, t^*)$, $u_b^*(x^*, y^*, t^*)$, $v_b^*(x^*, y^*, t^*)$, and at the sides of the brain by $p_s^*(x^*, y^*, t^*)$, $u_s^*(x^*, y^*, t^*)$, $v_s^*(x^*, y^*, t^*)$ respectively.

Estimates of the model parameter values are given in Table 1. Experimental data suggests typical shaking amplitudes of $20-50$ cm, and frequencies of $2-5$Hz [9].

3.1.1 Governing equations

The Navier-Stokes equations for fluid flow are given by

$$\frac{\partial u^*}{\partial x^*} + \frac{\partial v^*}{\partial y^*} = 0, \tag{14}$$

$$\rho_F^* \left(\frac{\partial u^*}{\partial t^*} + u^* \frac{\partial u^*}{\partial x^*} + v^* \frac{\partial u^*}{\partial y^*} \right) = -\frac{\partial p^*}{\partial x^*} + \mu^* \left(\frac{\partial^2 u^*}{\partial x^{*2}} + \frac{\partial^2 u^*}{\partial y^{*2}} \right), \tag{15}$$

$$\rho_F^* \left(\frac{\partial v^*}{\partial t^*} + u^* \frac{\partial v^*}{\partial x^*} + v^* \frac{\partial v^*}{\partial y^*} \right) = -\frac{\partial p^*}{\partial y^*} + \mu^* \left(\frac{\partial^2 v^*}{\partial x^{*2}} + \frac{\partial^2 v^*}{\partial y^{*2}} \right), \tag{16}$$

representing conservation of mass and x^*- and y^*- momentum respectively. These are applied to the back, side and front of the brain, denoted by subscript b, s and f respectively. Conservation of momentum on the brain relates the forcing from the shaking of the skull, $f^*(t^*) = A^* \cos(2\pi\omega^* t^*)$, to the CSF pressures at the front and back of the head

$$2\int_{-2L^*}^{-L^*} p_f^* \, \mathrm{d}x^* - 2\int_{L^*}^{2L^*} p_b^* \, \mathrm{d}x^* = 4\rho_B^* L^{*2} \frac{\mathrm{d}^2 f^*}{\mathrm{d}t^{*2}}, \tag{17}$$

where we exploit the inequality $A^* \gg h_0^*$.

We apply boundary conditions

$$u_f^* = v_f^* = 0 \quad \text{on} \quad y^* = 0, \ -2L^* \le x^* \le -L^*, \tag{18}$$

$$u_f^* = 0 \quad v_f^* = \frac{\mathrm{d}h^*}{\mathrm{d}t^*} \quad \text{on} \quad y^* = h_0^* + h^*, \ -2L^* \le x^* \le -L^*, \tag{19}$$

$$u_s^* = 0, \quad v_s^* = 0 \quad \text{on} \quad y^* = 0, \ -L^* \le x^* \le L^*, \tag{20}$$

$$u_s^* = \frac{\mathrm{d}h^*}{\mathrm{d}t^*}, \quad v_s^* = 0 \quad \text{on} \quad y^* = h_0^*, \ -L^* \le x^* \le L^*, \tag{21}$$

$$u_b^* = v_b^* = 0 \quad \text{on} \quad y^* = 0, \ L^* \le x^* \le 2L^*, \tag{22}$$

$$u_b^* = 0, \quad v_b^* = -\frac{\mathrm{d}h^*}{\mathrm{d}t^*} \quad \text{on} \quad y^* = h_0^* - h^*, \ L^* \le x^* \le 2L^*. \tag{23}$$

along with continuity of pressure and flux at the brain corners,

$$p_f^* = p_s^*, \quad \int_0^{h_0^*+h^*} u_f^* \mathrm{d}y^* = \int_0^{h_0^*} u_s^* \mathrm{d}y^* \quad \text{at} \quad x^* = -L^*, \tag{24}$$

$$p_b^* = p_s^*, \quad \int_0^{h_0^*} u_s \mathrm{d}y^* = \int_0^{h_0^*-h^*} u_b^* \mathrm{d}y^* \quad \text{at} \quad x^* = L^*, \tag{25}$$

and assume that there is symmetry in the sagittal plane,

$$\frac{\partial p_f^*}{\partial x^*} = 0 \quad \text{at} \quad x^* = -2L^*, \qquad \frac{\partial p_b^*}{\partial x^*} = 0 \quad \text{at} \quad x^* = 2L^*. \tag{26}$$

3.1.2 Nondimensionalisation

We consider the fluid motion on the timescale based on the shaking frequency, and introduce the nondimensionalisation

$$t^* = t/2\pi\omega^*,\ x^* = L^*x,\ y^* = \epsilon L^* y,\ h^* = \epsilon L^* h \tag{27}$$

$$p^* = p_0^* + P^* p,\ u^* = 2\pi\omega^* L^* u,\ v^* = 2\epsilon\pi\omega^* L^* v, \tag{28}$$

where (28) are all applied to the front, side and back of the brain, denoted by subscript f, b and s respectively. Here p_0^* is the reference pressure taken such that $p_s = 0$ at $t = 0$, $x = 0$, $\epsilon = h_0^*/L^* \ll 1$ is the aspect ratio and P^* is the pressure scaling to be determined. We have taken a convective velocity scaling, again based on the shaking frequency. We identify the dimensionless parameters

$$\mathrm{Re} = \frac{\rho_f^* 2\pi\omega^* L^{*2}}{\mu^*}, \quad \alpha = \frac{8\rho_B^* L^* \pi^2 \omega^{*2} A^*}{P^*}, \tag{29}$$

representing the ratio of inertial to viscous forces (the Reynolds number) and the ratio between shaking forces and those from the fluid pressure respectively.

Equations (14 - 17) become

$$\frac{\partial u}{\partial x} + \frac{\partial v}{\partial y} = 0, \tag{30}$$

$$\epsilon^2 \mathrm{Re}\left(\frac{\partial u}{\partial t} + u\frac{\partial u}{\partial t} + v\frac{\partial u}{\partial y}\right) = -\frac{P^*\epsilon^2}{2\mu^*\pi\omega^*}\frac{\partial p}{\partial x} + \epsilon^2\frac{\partial^2 u}{\partial x^2} + \frac{\partial^2 u}{\partial y^2}, \tag{31}$$

$$\epsilon^2 \mathrm{Re}\left(\frac{\partial v}{\partial t} + u\frac{\partial v}{\partial x} + v\frac{\partial v}{\partial y}\right) = -\frac{P^*}{2\mu^*\pi\omega^*}\frac{\partial p}{\partial y} + \epsilon^2\frac{\partial^2 v}{\partial x^2} + \frac{\partial^2 v}{\partial y^2}, \tag{32}$$

$$\int_{-2}^{-1} p_f \,\mathrm{d}x - \int_1^2 p_b \,\mathrm{d}x = -\alpha\cos t, \tag{33}$$

and boundary conditions (18 - 26) become

$$u_f = v_f = 0 \quad \text{on} \quad y = 0,\ -2 \le x \le -1, \tag{34}$$

$$u_f = 0 \quad v_f = \frac{\mathrm{d}h}{\mathrm{d}t} \quad \text{on} \quad y = 1 + h,\ -2 \le x \le -1, \tag{35}$$

$$u_s = 0, \quad v_s = 0 \quad \text{on} \quad y = 0,\ -2 \le x \le -1, \tag{36}$$

$$u_s = \epsilon\frac{\mathrm{d}h}{\mathrm{d}t}, \quad v_s = 0 \quad \text{on} \quad y = 1,\ -1 \le x \le 1, \tag{37}$$

$$u_b = v_b = 0 \quad \text{on} \quad y = 0,\ 1 \le x \le 2, \tag{38}$$

$$u_b = 0, \quad v_b = -\frac{\mathrm{d}h}{\mathrm{d}t} \quad \text{on} \quad y = 1 - h,\ 1 \le x \le 2, \tag{39}$$

$$p_f = p_s, \quad \int_0^{1+h} u_f \mathrm{d}y = \int_0^1 u_s \mathrm{d}y \quad \text{at} \quad x = -1, \tag{40}$$

$$p_b = p_s, \quad \int_0^1 u_s \mathrm{d}y = \int_0^{1-h} u_b \mathrm{d}y \quad \text{at} \quad x = 1, \tag{41}$$

$$\frac{\partial p_f}{\partial x} = 0 \quad \text{at} \quad x = -2, \qquad \frac{\partial p_b}{\partial x} = 0 \quad \text{at} \quad x = 2. \tag{42}$$

The choice of P^* depends on whether inertia or viscosity dominates the motion. If $\epsilon^2\mathrm{Re} \ll 1$, viscosity dominates, and we take

$$P^* = \frac{2\pi\omega^*\mu^*}{\epsilon^2}, \tag{43}$$

leading to the leading-order governing equations

$$-\frac{\partial p}{\partial x} + \frac{\partial^2 u}{\partial y^2} = 0, \tag{44}$$

$$\frac{\partial p}{\partial y} = 0, \tag{45}$$

along with (30, 33). In this case

$$\alpha = \alpha_v = \frac{4\rho_B^*\pi A^* h_0^{*2}\omega^*}{\mu^* L*}. \tag{46}$$

When $\mathrm{Re} \gg 1$, such that inertia dominates, with $\epsilon^2\mathrm{Re} = O(1) = \mathcal{R}$, we choose

$$P^* = \rho_F^* \left(2\pi\omega^* L^*\right)^2, \tag{47}$$

which gives the leading-order governing equations

$$\frac{\partial u}{\partial t} + u\frac{\partial u}{\partial x} + V\frac{\partial u}{\partial Y} = -\frac{\partial p}{\partial x} + \frac{\partial^2 u}{\partial Y^2}, \tag{48}$$

$$\frac{\partial p}{\partial Y} = 0, \tag{49}$$

upon scaling $v = V/\sqrt{\mathcal{R}}$, $y = Y/\sqrt{\mathcal{R}}$ along with (30, 33). These are the Prandtl boundary-layer equations [7], with an additional pressure coupling equation (33). In this case

$$\alpha = \alpha_I = \frac{2\rho_B^* A^*}{\rho_F^* L^*}. \tag{50}$$

Which regime is appropriate is determined by the reduced Reynolds number, $\epsilon^2\mathrm{Re}$, which can be expressed as

$$\epsilon^2\mathrm{Re} = \underbrace{2\pi\omega^*}_{\text{event dependent}} \times \underbrace{\frac{\rho_F^* h_0^{*2}}{\mu^*}}_{\text{physiological}}. \tag{51}$$

Using the values in Table 1 we find

$$\epsilon^2\mathrm{Re} = 2\pi\omega^*, \tag{52}$$

and hence for realistic shaking frequencies of $2 - 5\mathrm{Hz}$, $\epsilon^2\mathrm{Re} = O(1)$, and the inertia-dominated regime is the correct limit.

Due to time constraints we have not made analytical progress on the inertia-dominated dynamics. For completeness we now analyse the viscous-dominated regime. This will be the case for smaller shaking frequencies or thinner CSF layers.

3.2 Solution in a viscous-dominated regime

We now consider the viscous-dominated regime. Following the standard derivation of the squeeze-film equations [7] we may formulate the problem in terms of h and p_i for $i = f, s, b$, thus

$$\frac{\mathrm{d}h}{\mathrm{d}t} = (1+h)^3 \frac{\partial^2 p_f}{\partial x^2}, \tag{53}$$

$$-\frac{\mathrm{d}h}{\mathrm{d}t} = (1-h)^3 \frac{\partial^2 p_b}{\partial x^2}, \tag{54}$$

$$\frac{\partial^2 p_s}{\partial x^2} = 0, \tag{55}$$

$$\int_{-2}^{-1} p_f \,\mathrm{d}x - \int_{1}^{2} p_b \,\mathrm{d}x = -\alpha \cos t, \tag{56}$$

with boundary conditions

$$p_f = p_s, \quad \frac{\partial p_f}{\partial x}(1+h)^3 = \frac{\partial p_s}{\partial x} \quad \text{at} \quad x = -1, \tag{57}$$

$$p_b = p_s, \quad \frac{\partial p_b}{\partial x}(1-h)^3 = \frac{\partial p_s}{\partial x} \quad \text{at} \quad x = 1, \tag{58}$$

$$\frac{\partial p_f}{\partial x} = 0 \quad \text{at} \quad x = -2, \qquad \frac{\partial p_b}{\partial x} = 0 \quad \text{at} \quad x = 2. \tag{59}$$

The system (53 – 59) may be solved to find

$$p_f = \frac{1}{(1+h)^3}\frac{\mathrm{d}h}{\mathrm{d}t}\left(\frac{(x+2)^2}{2} + (1+h)^3 - \frac{1}{2}\right), \tag{60}$$

$$p_s = \frac{\mathrm{d}h}{\mathrm{d}t}x, \tag{61}$$

$$p_b = -\frac{1}{(1-h)^3}\frac{\mathrm{d}h}{\mathrm{d}t}\left(\frac{(x-2)^2}{2} - 3(1-h)^3 - \frac{1}{2}\right), \tag{62}$$

for the pressures $p_f(x,t)$, $p_s(x,t)$, $p_b(x,t)$, with the implicit expression for the perturbation to the CSF thickness, $h(t)$,

$$\alpha \sin(t) = 2h - \frac{1}{6(1+h)^3} + \frac{1}{6(1-h)^3}. \tag{63}$$

3.2.1 Results

We solve (63) using Matlab. Figure 5 shows how the relative brain displacement, $h(t)$, varies with time for a range of values of α. A larger α corresponds to a larger shaking force and therefore, as expected, the perturbations are larger. We note that because we used the lubrication-theory limit, $h(t)$ can never reach 1 (see (63)), and therefore the brain and skull can not actually touch. In Figure 4 we plot the fluid pressure around the brain at various time points for varying

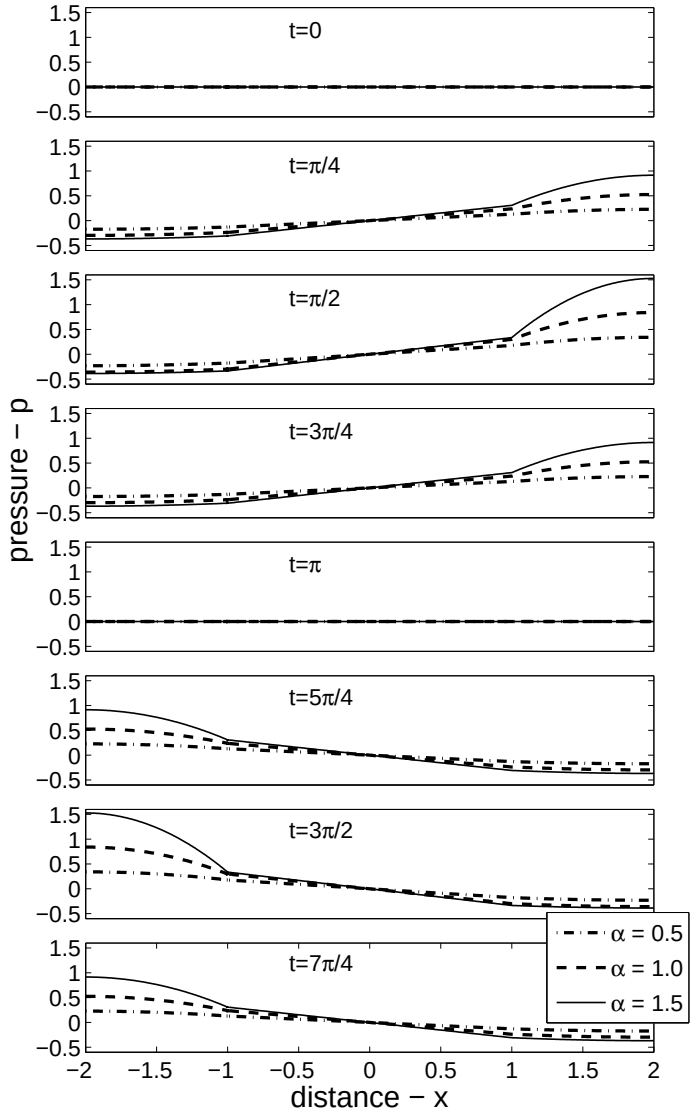

Figure 4: The pressure waves at various time points for varying α.

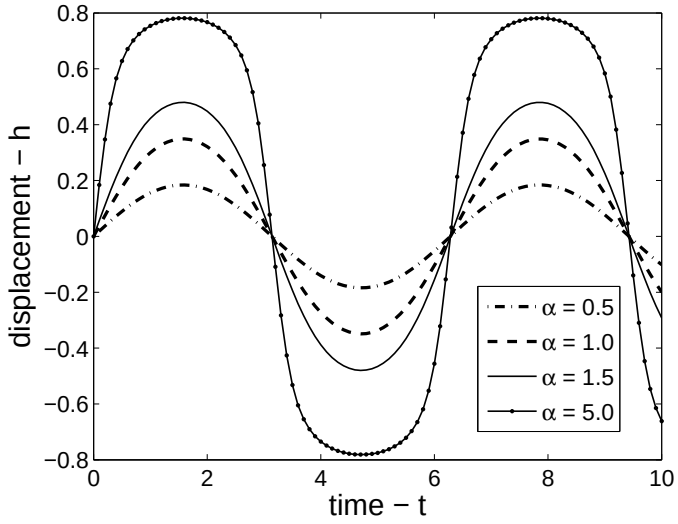

Figure 5: The relative brain displacement for a range of values of α.

α. For larger values of α, the CSF pressure in the compressed side of the head is significantly increased, potentially leading to more damage of the brain material.

The bridging vessels run between the brain and the skull, and will rupture if they are stretched by over 30%, and so the vessel at the front of the head will rupture if the maximum relative brain displacement, $h(t)$ is greater that 0.3. Therefore, from (63), the bridging vessels rupture if

$$\alpha = \frac{\pi \rho^* A^* \omega^* h_0^{*2}}{3\mu^* L^*} \gtrsim 1.01. \tag{64}$$

Figure 6 shows the range of shaking amplitudes and frequencies for which the model predicts vessel rupture, (64), using the parameter estimates given in Table 1. If the CSF layer is thicker (*i.e.* $h_0^* = 2\,\text{mm}$), there is a larger range of shaking amplitudes and frequencies that could cause significant vein rupture; therefore if a baby happens to have a thick CSF layer, shaken baby syndrome is more likely.

3.3 Discussion

We have derived the equations of motion for the CSF dynamics in two distinguished limits: viscous dominated (30, 33, 44, 45) and inertia dominated (30, 33, 48, 49). In the viscous-dominated regime, the model demonstrates that rupture of the bridging vessels due to brain movement is a physically plausible mechanism to explain shaken-baby syndrome. We predict vessel rupture if the key parameter α is above a threshold value, (64), and therefore, rupture

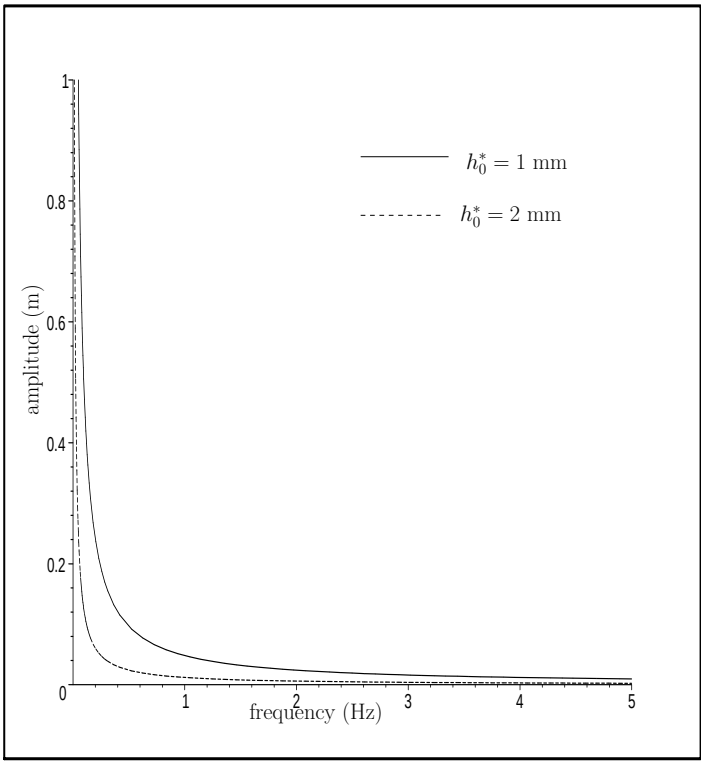

Figure 6: All values above the marked lines correspond to shaking amplitudes and frequencies that the model predicts will result in bridging-vessel rupture. The remaining parameter values are given in Table 1.

is more likely with a larger amplitude of shaking, an increased frequency of shaking, or if a baby has a thicker CSF layer. However, this analysis is not biologically relevant, as the viscous regime is inappropriate. Further analysis of the inertia-dominated regime would be necessary to see if the bridging vessels actually rupture during a shaking event.

In the model, we have made various simplifying assumptions, the validity of which could be investigated in future work. We assume that the bridging vessels do not provide any resistance to brain motion; however, it may be more appropriate to model the vessels as strings, with a simple Hookean law relating their extension to their tension. This model extension would create an extra term in the governing force-balance equation, (63), and reduce the range of shaking amplitudes and frequencies that cause vessel rupture. It would also be interesting to consider an incompressible elastic brain in this fluid model, and we could then investigate whether resonance is possible.

4 Conclusions

We have investigated two mechanisms for brain damage during shaking events; those caused by elastic effects within the brain and those caused by the presence of the thin layer of CSF between the brain and the skull.

For an elastic brain, a larger deformation was observed for rotational deformations than for longitudinal ones. Upon examining the frequencies at which resonance will occur, we found them to be in the range $7 - 10$ Hz, which are higher (though of the same order of magnitude) than those observed within a typical shaking event [9]. However, these calculations are highly dependent on the geometry involved, and so these estimates may be reduced when calculated with accurate geometry rather than the idealised sphere we have taken here.

When the dynamics of the CSF layer is considered (taking the brain and skull to both be rigid) we derived the equations of motion in two distinguished limits: viscous dominated (30, 33, 44, 45) and inertia dominated (30, 33, 48, 49). Which regime is appropriate is governed by the size of the reduced Reynolds number; (see equation (51)). This parameter can be considered to be the product of *i*) an event dependent parameter (a different shaking frequency can lead to a different response) and *ii*) a physiological parameter (different babies may have a varying response to the same shaking event).

The parameter α represents the importance of shaking forces and fluid pressure, and varies depending on regime; (46) in the viscous-dominated regime and (50) in the inertia-dominated regime. These expressions are related via

$$\alpha_v \quad = \quad \epsilon^2 \, \mathrm{Re} \, \alpha_I. \tag{65}$$

From Table 1, we expect $\alpha_I = O(1)$, and since the viscous-dominated limit is only valid when $\epsilon^2 \, \mathrm{Re} \ll 1$, we will always have $\alpha_v \ll 1$ when this parameter is relevant. In the viscous-dominated regime the coupling of the shaking to the CSF dynamics is always negligible, whilst in the inertia-dominated regime the shaking forces and fluid pressures are comparable and so coupling will occur.

From physiological values (Table 1) we see that $\epsilon^2 \mathrm{Re} = O(1)$, and so the correct limit is the inertia-dominated regime, with $\alpha_I = O(1)$. To enable progress, we analysed the less physically realistic viscous-dominated regime with $\alpha_v = O(1)$ to illustrate the mechanism. The analysis of the inertia-dominated system remains to be done.

References

[1] M. Abramowitz and I.A. Stegun. *Handbook of Mathematical Functions*. Dover, New York, 1965.

[2] T J David. Shaken baby (shaken impact) syndrome: non-accidental head injury in infancy. *J Roy Soc Med*, 92(11):556–61, 1999.

[3] P.D. Howell, G. Kozyreff, and J.R. Ockendon. *Applied Solid Mechanics*. Cambridge University Press, 2008.

[4] M. Hrapko, J.A.W. van Dommelen, G.W.M. Peters, and J.S.H.M. Wismans. The influence of test conditions on characterization of the mechanical properties of brain tissue. *J. Biomech. Eng.*, 130(3):031003, 2008.

[5] H.B. McClung. The elastic sphere under nonsymmetric loading. *J. Elasticity*, 21(1):1–26, 1989.

[6] H.B. McClung. Asymmetric vibrations of an elastic sphere. *J. Elasticity*, 25(1):75–94, 1991.

[7] H Ockendon and J.R Ockendon. *Viscous Flow*. CUP, 1995.

[8] A.C. Pipkin. *Lectures on Viscoelasticity Theory*. Springer-Verlag, New York, 1972.

[9] D R Wolfson, D S McNally, M J Cliford, and M Vloeberghs. Rigid-body modelling of shaken baby syndrome. *Proc. IMechE. Part H: J. Engineering in Medicine*, 219:63–70, 2005.